

Effective collision strengths for transitions in the $4p^k$ ($k = 2-4$) ground configurations of Kr III, Kr IV and Kr V

T. Schöning

Institut für Astronomie und Astrophysik der Universität München, Scheinerstr. 1, D-81679 München, Germany

Received June 13, accepted July 19, 1996

Abstract. Effective electron excitation collision strengths for fine-structure forbidden transitions within the $4p^k$ ($k = 2 - 4$) ground configurations of Kr III, Kr IV and Kr V have been calculated using the Breit-Pauli R-matrix technique and are tabulated in the range 2 000 – 50 000 K. The model for the system target + electron is based on a 6- (Kr III), 7- (Kr IV) and 8-state (Kr V) close-coupling representation. The comparison with the results of the semi-relativistic R-matrix method reveals the importance of full intermediate coupling especially at low electron temperatures. Our data will enable detailed quantitative analyses of collisionally excited krypton lines in the spectra of gaseous nebulae.

Key words: atomic data — plasmas — planetary nebulae: NGC 7027

1. Introduction

The recent detection of heavy trace elements with nuclear charge numbers $Z > 30$ in the planetary nebula (PN) NGC 7027 (Péquignot & Baluteau 1994, hereafter referred to as PB94) has opened up interesting scientific possibilities in astrophysics. In particular, several relatively strong collisionally excited forbidden lines in the [Kr III, IV, V] spectra were unambiguously identified. Using crude estimates for the collision strengths of krypton ions Péquignot & Baluteau found that krypton could be overabundant by a factor of ~ 20 compared to the solar system value. This unexpected result is a clear indication that PNe can play a much more important rôle in the overall process of element synthesis than has previously been recognized. Since the noble gas emerges from the neutron capture process in the interior of the progenitor of NGC 7027 and has obviously been injected into the interstellar medium it is very interesting with a view to testing models for the final

stages of stellar evolution and the chemical evolution of galaxies.

We have tackled the problem of calculating collisional data for krypton ions. In a previous paper (Schöning & Butler 1995, hereafter referred to as Paper I) we have provided for the first time effective collision strengths for fine-structure forbidden transitions in the $4p^3$ ground configuration of Kr IV. Since this ion was considered as a test case for the computation of collisional data for heavy elements the scattering problem was solved using a semi-relativistic R-matrix approach, i.e. the method approximately allows for relativistic effects in the target through transformations of the LS-coupling transmission matrices calculated with the non-relativistic R-matrix technique (Berrington et al. 1987) to intermediate coupling. Nevertheless, we have argued that this method yields reliable results which lead us to conclude that the krypton overabundance reported by Péquignot & Baluteau is probably real.

However, convincing quantitative analyses of the observed lines make it necessary to employ the most accurate collisional data currently achievable. Thus the aim of this paper is to apply recently developed electron scattering techniques to the calculation of collision strengths for krypton ions such that relativistic effects in both the target and scattered electron wave function are consistently included from the outset. Within the context of the R-matrix method two approaches are available. In the low- Z Breit-Pauli (BP) formulation (see Hummer et al. 1993, hereafter IP93) the non-relativistic continuum Hamiltonian is transformed from LS coupling to a pair coupling scheme and the one-body mass correction, Darwin and spin-orbit terms are additionally included. However, since it is well known that the BP Hamiltonian is applicable to intermediate Z -ions with Z not much beyond $Z = 30$ test calculations are desirable for at least one of the krypton ($Z = 36$) ions using the Dirac R-matrix theory (see Norrington & Grant 1987) which is the state of art for the heavy-atom case. These calculations are currently underway and will be the subject of a future paper (Schöning, in preparation).

The plan of this paper is as follows. In Sect. 2 we outline the calculation of effective collision strengths for the ions of krypton under consideration. The results are presented in Sect. 3 and critically discussed in Sect. 4. Finally, concluding remarks are given in Sect. 5.

2. Calculations

Since a consistent treatment of relativistic effects in both the target and scattered electron wavefunction is computationally demanding it is necessary to keep the dimensions of the problem to a reasonably small level. Thus the total wavefunction for the system target + electron was calculated in a 6- (Kr III), 7- (Kr IV) and 8-state (Kr V) close-coupling representation. In Table 1 we list the spectroscopic target configurations along with a number of correlation configurations included essentially for improving the target energies. For transitions within the $4p^k$ ($k = 2, 3, 4$) ground configurations these target representations allow for sufficient collisional coupling with higher target states for the electron temperatures (and energies) under consideration. The SUPERSTRUCTURE package (Eissner et al. 1974; Nussbaumer & Storey 1978) has been employed to optimize the one-electron orbitals nl . The corresponding adjustable scaling parameters λ_{nl} in the statistical-model potential are to be found in Table 2. Subsequently Table 3 shows the calculated fine-structure energy levels together with the observed values taken from Sugar & Musgrove (1991). Except for the lowest states the relative difference between theory and experiment is generally much less than 10%. The case of the Kr III and Kr V 3P ground term fine-structure states is marginal since the absolute deviations in the fine-structure energy splittings are similar to those of higher states. With regard to the first excited $^2D^o$ term in Kr IV the agreement could be further improved through the inclusion of, for example, $4f$ pseudo-orbitals. However, the corresponding pseudo-resonances in the collision strengths are located close to threshold and could significantly contribute to the thermally averaged collision strengths leading to inaccurate results. Finally, for selected transitions SUPERSTRUCTURE gf values calculated in the length and velocity formulations are given in Table 4. The agreement is reasonable considering the rather coarse description of the complex targets. We note that in the scattering calculations the theoretical energy levels have been replaced by those measured such that the target thresholds are adjusted to the correct values.

The scattering calculations have been performed using two different approaches of various sophistication for the collisional problem with the inclusion of relativistic effects. These methods are based on: (a) purely algebraic recoupling of LS target terms to an LSJ coupling scheme and $J - J$ coupling between target terms using term coupling coefficients (TCC's) and (b) full intermediate coupling calculation using the BP Hamiltonian for electron-ion scat-

Table 1. Configurations included in the target representations. All configurations include $1s^2 2s^2 2p^6 3s^2 3p^6 3d^{10}$

Kr III	Kr IV	Kr V
$4s^2 4p^4$	$4s^2 4p^3$	$4s^2 4p^2$
$4s^2 4p^3 4d$	$4s^2 4p^2 4d$	$4s^2 4p 4d$
$4s^2 4p^2 4d^2$	$4s^2 4p 4d^2$	$4s^2 4d^2$
$4s^2 4p 4d^3$	$4s 4p^4$	$4s 4p^3$
$4s 4p^5$	$4s 4p^3 4d$	$4s 4p^2 4d$
$4s 4p^4 4d$	$4s 4p^2 4d^2$	$4s 4p 4d^2$
$4s 4p^3 4d^2$	$4p^5$	$4p^4$
$4p^6$	$4p^4 4d$	$4p^3 4d$
$4p^5 4d$	$4p^3 4d^2$	$4p^2 4d^2$
$4p^4 4d^2$		

Table 2. Values for the adjustable scaling parameters λ_{nl} in the statistical-model potential used to calculate the one-electron orbitals

	Kr III	Kr IV	Kr V
λ_{1s}	1.4230	1.4223	1.4214
λ_{2s}	1.1386	1.1375	1.1380
λ_{2p}	1.0849	1.0843	1.0837
λ_{3s}	1.0379	1.0351	1.0371
λ_{3p}	1.0201	1.0199	1.0173
λ_{3d}	0.9997	0.9997	0.9989
λ_{4s}	0.9891	0.9898	0.9907
λ_{4p}	0.9994	0.9987	0.9962
λ_{4d}	1.0622	1.0920	1.0830

tering. We begin with approximation (a) which has been discussed in Paper I. Here the solution of the collisional problem is efficiently achieved in LS -coupling by means of the Iron Project version of the R-matrix package (IP93) where the hamiltonian is taken to be the non-finestructure part H_{nfs} of the low- Z Breit-Pauli hamiltonian

$$H_{nfs} = H_{NR} + H_{mass} + H_{Dar} \quad (1)$$

with H_{NR} being the usual non-relativistic Hamiltonian. H_{mass} and H_{Dar} denote the one-body mass correction and Darwin term respectively. These relativistic operators yield important energy corrections to the N -electron target and $(N + 1)$ -electron intermediate bound states. Then the calculation of collision strengths for transitions between fine-structure target levels essentially involves an algebraic transformation of the transmission matrices ($T = 1 - S$) to intermediate coupling. Following Saraph (1978) relativistic effects are included to first order through a further transformation of the T-matrices using term-coupling coefficients. The latter are obtained as by-products in a BP run of the RAL version of the Iron Project

Table 3. Observed (Sugar & Musgrove) and calculated Kr III, Kr IV and Kr V fine-structure energy levels in Ryd

Kr III	Obs.	Calc.	Kr IV	Obs.	Calc.	Kr V	Obs.	Calc.
$4s^2 4p^4 \ ^3P_2$	0.0	0.0	$4s^2 4p^3 \ ^4S_{3/2}$	0.0	0.0	$4s^2 4p^2 \ ^3P_0$	0.0	0.0
$\ ^3P_1$	0.04145	0.03462	$\ ^2D_{3/2}^o$	0.15525	0.18550	$\ ^3P_1$	0.03411	0.02582
$\ ^3P_0$	0.04841	0.04264	$\ ^2D_{5/2}^o$	0.17041	0.19640	$\ ^3P_2$	0.06921	0.05686
$\ ^1D_2$	0.13345	0.14514	$\ ^2P_{1/2}^o$	0.28300	0.30821	$\ ^1D_2$	0.17973	0.18540
$\ ^1S_0$	0.30144	0.30196	$\ ^2P_{3/2}^o$	0.30441	0.32224	$\ ^1S_0$	0.35725	0.36628
$4s4p^5 \ ^3P_2^o$	1.05644	1.02339	$4s4p^4 \ ^4P_{5/2}$	1.08222	1.05507	$4s4p^3 \ ^3D_1^o$	1.18153	1.14560
$\ ^3P_1^o$	1.08787	1.05073	$\ ^4P_{3/2}$	1.11563	1.08244	$\ ^3D_2^o$	1.18264	1.14597
$\ ^3P_0^o$	1.10758	1.06663	$\ ^4P_{1/2}$	1.13097	1.09595	$\ ^3D_3^o$	1.19391	1.15333
$\ ^1P_1^o$	1.29287	1.30146	$\ ^2D_{3/2}$	1.32837	1.33697	$\ ^3P_0^o$	1.34799	1.31788
$4s^2 4p^3 4d \ ^5D_0^o$	1.26162	1.27483	$\ ^2D_{5/2}$	1.33632	1.34142	$\ ^3P_1^o$	1.35129	1.31963
$\ ^5D_1^o$	1.26184	1.27599	$\ ^2P_{3/2}$	1.48941	1.54404	$\ ^3P_2^o$	1.35477	1.31909
$\ ^5D_2^o$	1.26193	1.27807	$\ ^2P_{1/2}$	1.51416	1.56237	$\ ^1D_2^o$	1.48889	1.48923
$\ ^5D_3^o$	1.26204	1.28065	$\ ^2S_{1/2}$	1.58516	1.61051	$\ ^3S_1^o$	1.68642	1.72922
$\ ^5D_4^o$	1.26346	1.28320				$\ ^1P_1^o$	1.76823	1.80940

Table 4. Comparison of selected SUPERSTRUCTURE gf values calculated in the length (L) and velocity (V) formulations for the Kr III, Kr IV and Kr V ions

Kr III			Kr IV			Kr V		
Transition	L	V	Transition	L	V	Transition	L	V
$\ ^1D_2-^1P_1^o$	0.168	0.0492	$\ ^2D_{5/2}^o-^2P_{3/2}$	0.537	0.332	$\ ^3P_2-^3S_1^o$	2.03	1.70
$\ ^3P_2-^3P_2^o$	0.120	0.0920	$\ ^2D_{5/2}^o-^2D_{5/2}$	0.381	0.335	$\ ^1D_2-^1P_1^o$	1.85	1.37
$\ ^3P_2-^3P_1^o$	0.0415	0.0291	$\ ^2D_{3/2}^o-^2D_{3/2}$	0.289	0.254	$\ ^3P_1-^3S_1^o$	1.08	0.885
$\ ^3P_1-^3P_2^o$	0.0394	0.0327	$\ ^2P_{3/2}^o-^2S_{1/2}$	0.268	0.193	$\ ^1D_2-^1D_2^o$	0.853	0.688
$\ ^3P_1-^3P_0^o$	0.0302	0.0213	$\ ^2D_{3/2}^o-^2P_{1/2}$	0.256	0.160	$\ ^3P_2-^3P_2^o$	0.410	0.386
$\ ^3P_0-^3P_1^o$	0.0292	0.0220	$\ ^4S_{3/2}^o-^4P_{5/2}$	0.229	0.264	$\ ^3P_0-^3S_1^o$	0.399	0.317
$\ ^3P_1-^3P_1^o$	0.0228	0.0170	$\ ^4S_{3/2}^o-^4P_{3/2}$	0.149	0.159	$\ ^1S_0-^1P_1^o$	0.311	0.292
$\ ^1D_2-^3P_2^o$	0.00246	0.00264	$\ ^2P_{1/2}^o-^2P_{1/2}$	0.110	0.0907	$\ ^3P_2-^3D_3^o$	0.300	0.318
$\ ^3P_2-^1P_1^o$	0.00185	0.00017	$\ ^2P_{3/2}^o-^2D_{5/2}$	0.0883	0.107	$\ ^3P_1-^3D_2^o$	0.216	0.219
$\ ^3P_2-^5D_2^o$	0.00170	0.00204	$\ ^4P_{3/2}^o-^4P_{1/2}$	0.0747	0.0769	$\ ^3P_1-^1P_1^o$	0.203	0.156

R-matrix package (Eissner, private communication). As the TCC method neglects the fine-structure energy splitting of the target terms the effective collision strengths prove to be useful for higher temperatures such that the dominant contributions to the thermal average arise from collision energies above the fine-structure thresholds.

The more elaborate technique (b) used in this paper is based on the BP formulation of the R-matrix method (IP93). Here a consistent treatment of relativistic effects in both the target and scattered electron wavefunction is enabled through the use of the low- Z BP Hamiltonian

$$H_{BP} = H_{nfs} + H_{so} \quad (2)$$

which beside the non-finestructure part H_{nfs} (see Eq. (1)) contains the spin-orbit interaction H_{so} . The latter does not preserve LS symmetry but is diagonal in the total angular

momentum $J = L + S$. Accordingly the matrix elements of the BP Hamiltonian are most conveniently evaluated in a pair coupling scheme with explicit consideration of all scattering channels including fine structure. Thus the size of the Hamiltonian matrices and, consequently, the computing time greatly exceed that of the TCC calculations. The numerical solution is handled using the QUB version of the Iron Project R-matrix package (IP93) followed by a run of the Opacity Project asymptotic region code STGF (Berrington et al. 1987).

Partial waves have been included for all total angular momenta and parity symmetries with $J \leq 12$ which ensure sufficient convergence of the collision strengths for forbidden transitions within the target ground configuration. Due to the rather narrow resonance structure of the collision strengths we have set up the energy mesh

Table 5. Effective collision strengths for Kr III, IV, V. The left-hand column indicates the values of the electron temperature (Kelvin). In the row containing the ion symbol the indices of the initial and final levels are coded as follows:

Kr III 1. 3P_2 2. 3P_1 3. 3P_0 4. 1D_2 5. 1S_0
 Kr IV 1. $^4S_{3/2}$ 2. $^2D_{3/2}^o$ 3. $^2D_{5/2}^o$ 4. $^2P_{1/2}^o$ 5. $^2P_{3/2}^o$
 Kr V 1. 3P_0 2. 3P_1 3. 3P_2 4. 1D_2 5. 1S_0

Kr III	1-2	1-3	1-4	1-5	2-3	2-4	2-5	3-4	3-5	4-5
2000	3.794	0.819	2.501	0.220	1.505	1.691	0.215	0.566	0.063	1.603
4000	3.613	0.827	2.500	0.230	1.413	1.682	0.219	0.564	0.065	1.696
6000	3.512	0.833	2.479	0.258	1.360	1.667	0.234	0.560	0.073	1.788
8000	3.450	0.839	2.455	0.291	1.322	1.653	0.252	0.555	0.082	1.855
10000	3.419	0.849	2.436	0.321	1.293	1.640	0.268	0.551	0.090	1.898
12000	3.414	0.864	2.423	0.346	1.272	1.631	0.282	0.548	0.097	1.925
14000	3.426	0.882	2.416	0.367	1.257	1.625	0.293	0.546	0.102	1.939
16000	3.450	0.901	2.415	0.383	1.247	1.623	0.301	0.546	0.107	1.945
18000	3.481	0.921	2.419	0.396	1.241	1.623	0.309	0.546	0.110	1.946
20000	3.516	0.940	2.427	0.406	1.237	1.625	0.315	0.548	0.114	1.943
50000	3.964	1.126	2.749	0.450	1.262	1.799	0.362	0.610	0.142	1.867
Kr IV	1-2	1-3	1-4	1-5	2-3	2-4	2-5	3-4	3-5	4-5
2000	4.042	3.079	1.279	1.352	5.641	2.168	2.710	2.420	4.612	2.486
4000	3.397	3.521	1.211	1.341	5.904	2.089	3.061	2.458	4.771	2.665
6000	3.200	3.839	1.117	1.279	5.946	2.011	3.209	2.469	4.773	2.747
8000	3.117	4.046	1.036	1.224	5.865	1.958	3.276	2.460	4.760	2.778
10000	3.061	4.162	0.977	1.189	5.738	1.926	3.307	2.445	4.750	2.784
12000	3.008	4.211	0.936	1.173	5.602	1.910	3.319	2.428	4.747	2.777
14000	2.954	4.215	0.908	1.168	5.476	1.905	3.320	2.410	4.750	2.764
16000	2.898	4.189	0.890	1.171	5.365	1.908	3.316	2.393	4.758	2.748
18000	2.841	4.146	0.878	1.179	5.272	1.916	3.307	2.377	4.772	2.732
20000	2.785	4.093	0.870	1.188	5.195	1.927	3.298	2.362	4.789	2.718
50000	2.185	3.286	0.842	1.300	4.855	2.102	3.145	2.226	5.098	2.649
Kr V	1-2	1-3	1-4	1-5	2-3	2-4	2-5	3-4	3-5	4-5
2000	1.222	1.614	0.837	0.191	5.768	2.210	0.634	4.262	1.361	2.144
4000	1.550	1.707	0.919	0.194	6.684	2.603	0.651	4.974	1.341	1.936
6000	1.803	1.711	0.985	0.199	6.885	2.886	0.665	5.446	1.324	1.941
8000	1.937	1.697	1.020	0.204	6.861	3.047	0.676	5.714	1.310	2.025
10000	2.002	1.684	1.035	0.208	6.788	3.131	0.686	5.854	1.304	2.132
12000	2.032	1.675	1.039	0.212	6.710	3.170	0.698	5.923	1.303	2.237
14000	2.045	1.668	1.037	0.216	6.639	3.186	0.709	5.954	1.305	2.330
16000	2.049	1.662	1.032	0.219	6.576	3.190	0.719	5.965	1.307	2.409
18000	2.049	1.657	1.026	0.222	6.519	3.188	0.728	5.965	1.309	2.475
20000	2.046	1.652	1.019	0.224	6.468	3.181	0.736	5.958	1.310	2.527
50000	1.973	1.555	0.912	0.219	5.910	2.969	0.717	5.570	1.180	2.650

in terms of the effective quantum number ν relative to the next higher target threshold. It has been found that a step width $\Delta\nu = 0.0005$ gives good resolution of the resonances. Close to thresholds where the effective quantum number exceeds a value of $\nu_{\max} \approx 10$ Gailitis averaging (Gailitis 1963) of the resonances is performed and a constant interval length $\Delta E \approx 1 \cdot 10^{-5}$ Ryd in (z -scaled) energy is used.

3. Results

With regard to astrophysical applications it is convenient to calculate the effective collision strength Υ_{ij} which is the thermal average of the collision strength Ω_{ij}

$$\Upsilon_{ij} = \int_0^\infty \Omega_{ij}(x) \exp(-x) dx \quad (3)$$

where $x = E/k_B T$. E denotes the kinetic energy of the outgoing electron, T the electron temperature in Kelvin and $k_B = 6.339 \cdot 10^{-6}$ Ryd/K, the Boltzmann constant. Υ_{ij} enters into the excitation rate coefficient from level i to j through

$$q_{ij} = \frac{8.631 \cdot 10^{-6}}{g_i T^{1/2}} \exp\left(-\frac{E_{ij}}{k_B T}\right) \Upsilon_{ij} \text{ cm}^3 \text{ s}^{-1} \quad (4)$$

where g_i is the statistical weight of level i and E_{ij} the energy difference between levels i and j in Ryd. The de-excitation rate coefficient is given by

$$q_{ji} = \frac{8.631 \cdot 10^{-6}}{g_j T^{1/2}} \Upsilon_{ij} \text{ cm}^3 \text{ s}^{-1}. \quad (5)$$

In Table 5 we have tabulated Υ_{ij} for all transitions within the ground configurations of Kr III, IV, V and temperatures

ranging from 2000 to 50 000 K. This temperature grid is especially suitable for the modelling of gaseous nebulae and stellar atmospheres.

4. Discussion

We have used various R-matrix techniques for the calculation of collision strengths: the semi-relativistic TCC and the full intermediate coupling BP method. It is interesting to compare the collision strengths as a function of colliding electron energy obtained with the different approaches. This comparison demonstrates the influence of the consistent treatment of relativistic effects in the system target + electron on the effective collision strengths. Here we focus on selected Kr III, IV, V transitions from the ground state to excited states within the $4p^k$ ground configurations.

The collision strength of the $^3P_2 - ^3P_0$ fine-structure transition in Kr III is dominated by complex resonance structures at low electron energies (Fig. 1a). The position and shape of the resonances close to threshold clearly affect the effective collision strengths especially at low temperatures. In the BP calculation the threshold is not at zero energy due to fine-structure splitting whereas in the TCC method the fine-structure thresholds are assumed to be degenerate. The effect of the full relativistic approach is well reflected in the effective collision strength (Fig. 2a). In particular, for a temperature of 2000 K BP yields an effective collision strength which is 30% lower compared to TCC. The difference reduces with increasing temperature (10% at 10 000 K) and both methods agree in the high temperature limit as expected.

As to the $^4S_{3/2}^o - ^2D_{3/2}^o$ transition in Kr IV the BP calculation exhibits a remarkable Rydberg series of resonances in the collision strength at low energies (Fig. 1b). The series is converging to the $^2P_{1/2}^o$ threshold and superimposed on a broad resonance associated with bound channels in the $J = 4$ partial wave of even symmetry. Again the effect of fine-structure splitting can be clearly seen at the excitation threshold. Hence it is not surprising that the BP effective collision strength exceeds the TCC result by almost a factor of 2 at a temperature of 2000 K (Fig. 2b). However, the deviations rapidly diminish with increasing temperature such that the TCC results approach the BP values for $T > 15\,000$ K.

Finally, Fig. 1c demonstrates the collision strength for the $^3P_0 - ^1S_0$ transition in Kr V where similarly to the case of Kr IV the lowering of the collisional background close to threshold is prominent in the BP calculation. Moreover the comparison exhibits an important feature of the BP calculations, the shift of resonances due to relativistic spin-orbit effects on collisional complex terms. Accordingly the BP effective collision strength is much lower (35% at 2000 K) as compared to TCC (Fig. 2c).

To our knowledge experimentally measured collision strengths are not available for any krypton ions. Were the krypton abundances in NGC 7027 known we could infer

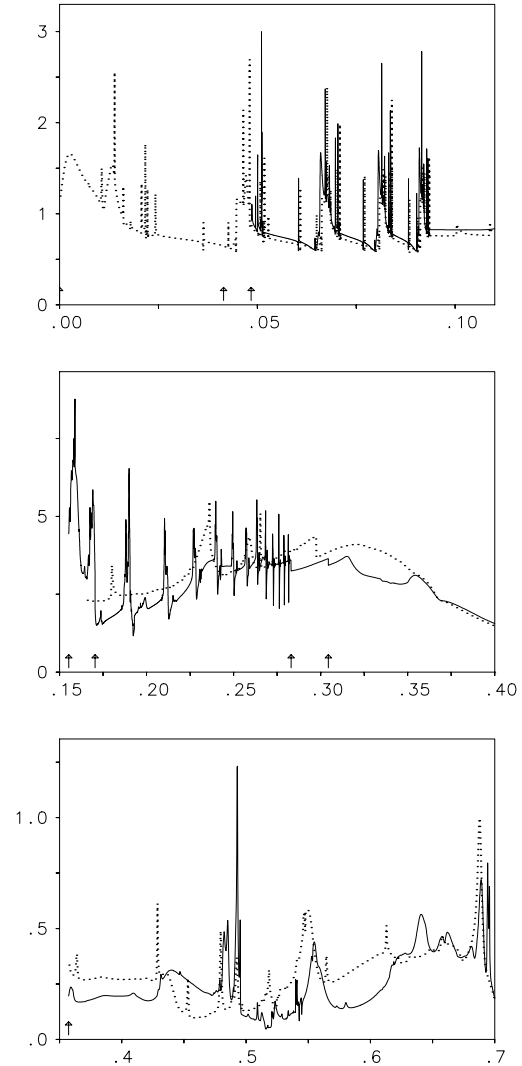


Fig. 1. Collision strength Ω as a function of the incoming electron energy (Ryd) in the near threshold region of the **a)** Kr III $^3P_2 - ^3P_0$, **b)** Kr IV $^4S_{3/2}^o - ^2D_{3/2}^o$ and **c)** Kr V $^3P_0 - ^1S_0$ transitions (full curve: BP, dotted: TCC method). The arrows on the energy axis mark the target fine-structure threshold energies

the effective collision strengths from the parameters Θ_λ in Tables 10–13 of PB94 which have been determined from the observed line intensities. It has been shown in PB94 that

$$\Theta_\lambda \propto \frac{n_{\text{ion}}}{n_{\text{elem}}} \Upsilon_{1j} \quad (6)$$

with n_{ion} being the actual nebular abundance of the ion emitting the line and n_{elem} the solar system elemental abundance relative to hydrogen. Υ_{1j} is the effective collision strength for the transition from the ground state to the upper level j of the line $j \rightarrow i$. Since abundances

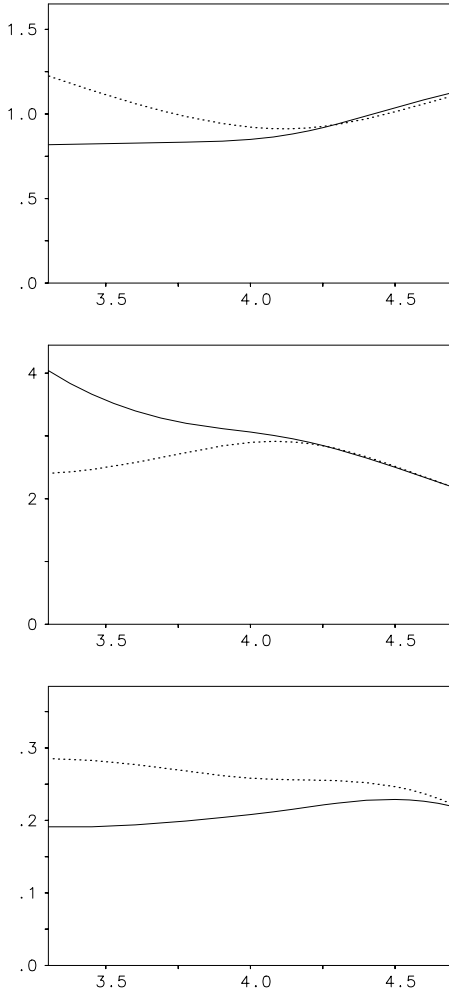


Fig. 2. Effective collision strength Υ as a function of $\log T$ (Kelvin) for the transitions **a)** Kr III $3P_2-3P_0$, **b)** Kr IV $4S_{3/2}^o-2D_{3/2}^o$ and **c)** Kr V $3P_0-1S_0$ (full curve: BP, dotted: TCC method)

are not known a priori we consider proper ratios of Θ_λ parameters, e.g.

$$\frac{\Theta_{5346}}{\Theta_{5868}} = \frac{\Upsilon_{13}}{\Upsilon_{12}} \quad (7)$$

for transitions in the Kr IV $4S-2D$ multiplet at 5868.0 Å (1–2) and 5346.1 Å (1–3). The labelling of the transitions in braces refers to the indices of the fine structure energy levels in Table 5. For a nebular temperature of 13 500 K (see Table 2 in PB94) the TCC and BP calculations yield $\Upsilon_{13}/\Upsilon_{12} = 1.42$ which is well within the error limit of the measurements ($\Theta_{5346}/\Theta_{5868} = 1.36 \pm 0.09$) of Péquignot & Baluteau. We note that agreement could not be achieved with a non-relativistic approach where the collision strengths for excitation from the $4S_{3/2}$ ground state to the individual $2D_{3/2,5/2}$ fine-structure levels are obtained from LS coupling data using statistical weights

and thus satisfy the relation $\Upsilon_{13}/\Upsilon_{12} = 1.5$. This result clearly demonstrates the importance of relativistic effects on the electron excitation of krypton ions.

On the other hand the Θ_λ parameters prove to be useful for determining the krypton abundance in NGC 7027. In their analysis (PB94) Péquignot & Baluteau tentatively presumed that collision strengths are similar for homologous forbidden transitions in Ar^{n+} and Kr^{n+} ions. However, by comparing our collision strengths for Kr III–V with the results of previous calculations for Ar III–V (Johnson & Kingston 1990; Zeppen et al. 1987; Mendoza 1983) we found that some effective collision strengths for Kr^{n+} are larger by more than a factor of 2 compared to Ar^{n+} . Consequently it is interesting to reanalyse the spectral data of PB94 and apply our new collision strengths for krypton ions.

We follow the method of PB94 except that we do not neglect the individual behaviour of the complex ions in collisional processes. Then for homologous transitions in argon and krypton ions we consider the ratio

$$y_n = \frac{\Theta_\lambda(Kr^{n+})}{\Theta_\lambda(Ar^{n+})} \quad (8)$$

and using (6) we rewrite (8) as

$$y_n = \frac{Kr^{n+}/Ar^{n+}}{Kr/Ar} \frac{\Upsilon_{1j}(Kr^{n+})}{\Upsilon_{1j}(Ar^{n+})}. \quad (9)$$

We emphasize that Kr^{n+}/Ar^{n+} denotes the ratio of ionic abundances in NGC 7027 and Kr/Ar is the ratio of solar system elemental abundances. In Table 6 y_n derived from the Θ_λ values in Tables 10–13 of PB94 are listed for selected homologous transitions in Ar^{n+} and Kr^{n+} ($n = 2, 3, 4$) ions. The transitions have been chosen such that for a specific ion number the uncertainty of Θ_λ quoted in PB94 is minimal.

The nebular abundance of krypton $n_{Kr,7027}$ in units of the solar system abundance $n_{Kr,\odot}$ (see Table 3 in PB94) is then given as

$$\frac{n_{Kr,7027}}{n_{Kr,\odot}} = icf \times \left(\sum_{n=1}^4 x_n y_n z_n \right) \quad (10)$$

where $x_n = Ar^{n+}/Ar$ is the ionization fraction of argon obtained from recent photoionization models of NGC 7027 (see Table 17 in PB94). The ratios of effective collision strengths $z_n = \Upsilon_{1j}(Ar^{n+})/\Upsilon_{1j}(Kr^{n+})$ have been calculated for electron temperatures according to Table 2 in PB94. The “ionization correction factor” icf (see Table 17 in PB94) accounts for contributions of unobserved highly ionized Ar^{n+} and Kr^{n+} ($n \geq 5$) ions to the sum in (10). No data are available for Ar^+ and Kr^+ , thus $y_1 z_1 = (Kr^+/Ar^+)/(Kr/Ar)$ is set arbitrarily to unity as these ions are negligible.

Using (10) and the values of x_n , y_n and z_n listed in Table 6 we find that krypton is overabundant in NGC 7027

Table 6. Homologous transitions in Arⁿ⁺ and Krⁿ⁺ ions used for determining the krypton abundance in NGC 7027

Ion number	II	III	IV	V
Transition		³ P ₂ ⁻¹ D ₂	⁴ S _{3/2} ^o - ² D _{5/2} ^o	³ P ₁ ⁻¹ D ₂
$\Upsilon_{1j}(\text{Ar}^{n+})/\Upsilon_{1j}(\text{Kr}^{n+})$	—	1.2	0.4	0.4
$(\Theta_{\lambda}(\text{Kr}^{n+})/\Theta_{\lambda}(\text{Ar}^{n+}))^a$	—	3.	35.4	13.5
$(\text{Ar}^{n+}/\text{Ar})^b$	3%	41%	21%	9%

^a Ratios determined from Θ_{λ} values in Tables 10-13 of PB94.

^b Ionic fractions of Ar from Table 17 of PB94.

by a factor of ~ 8 relative to the solar system value. We note that our result is lower by a factor of ~ 2 compared to the estimate of PB94. This is mainly due to the use of our calculated collision strength for the Kr IV ⁴S_{3/2}^o-²D_{5/2}^o transition which exceeds that of the homologous transition in Ar IV by more than a factor of 2.

5. Conclusion

This paper presents for the first time effective collision strengths for fine-structure forbidden transitions in the ground configurations of the 4p^k ions Kr III, IV, V obtained with the BP R-matrix approach. The comparison with the semi-relativistic TCC method, essentially an algebraic recoupling technique using term-coupling coefficients, reveals that the effects of full intermediate coupling manifest themselves most strongly at low electron temperatures where the two methods differ by up to a factor of 2. However, for higher temperatures ($T > 10\,000$ K) both methods generally agree to within 20%. Considering analyses of collisionally excited lines of krypton ions in PNe with high nebular temperatures these deviations are comparable with other uncertainties, e.g. due to the determination of ionization equilibria for heavy elements. Thus we conclude that for present diagnostics of nebular spectra the semi-relativistic method can be an adequate alternative to the computationally expensive BP calculations.

We have reanalysed the spectroscopic data of PB94 for NGC 7027 using our calculated collision strengths for the krypton ions. Our results confirm, although to a lesser extent, the enrichment of krypton in the nebula. The question concerning the mechanisms of the effective enhancement of the heavy element in the atmosphere of the progenitor of NGC 7027 is still open for discussion and will stimulate new strategies in the models of nucleosynthesis and stellar evolution. We note that our data will also be very useful for spectral analyses of other PNe and probably H II regions where lines of krypton ions may be detected with improved observational equipment.

Our future efforts will focus on the application of the Dirac R-matrix method to the calculation of collision strengths for at least one of the krypton ions. This investigation will make possible further checks of the accuracy of the present data. Collision strengths for other ions of astrophysical interest (Xe, Ba, Ni) will be available in the near future.

Acknowledgements. I would like to thank Dr. K. Butler for his continued support of this work and Dr. W. Eissner for making his RAL version of the Breit-Pauli R-matrix package available to us. I am also indebted to the Deutsche Forschungsgemeinschaft for financial support under grant Bu 703/2-1. The calculations were performed on the Cray Y-MP and HP 735 cluster of the Bayerische Akademie der Wissenschaften at the Leibniz Rechenzentrum, München. We gratefully acknowledge a grant of computer time by Cray Research Inc. in cooperation with the Leibniz Rechenzentrum.

References

- Berrington K.A., Burke P.G., Butler K., et al., 1987, J. Phys. B: At. Mol. Phys. 20, 6379
Eissner W., Jones M., Nussbaumer H., 1974, Comp. Phys. Commun. 8, 270
Gailitis M., 1963, Sov. Phys.-JETP 17, 1328
Hummer D.G., Berrington K.A., Eissner W., et al., 1993, A&A 279, 298 (IP93)
Johnson C.T., Kingston A.E., 1990, J. Phys. B: At. Mol. Opt. Phys. 23, 3393
Mendoza C., 1983, Physical Processes in Planetary Nebulae. In: Flower D.R. (ed.) IAU Symp. No. 103, Planetary Nebulae. Reidel, Dordrecht, p. 143
Norrington P.H., Grant I.P., 1987, J. Phys. B: At. Mol. Phys. 20, 4869
Nussbaumer H., Storey P.J., 1978, A&A 64, 139
Péquignot D., Baluteau J.-P., 1994, A&A 283, 593 (PB94)
Saraph H.E., 1978, Comp. Phys. Commun. 15, 247
Schöning T., Butler K., 1995, A&A 296, L29 (Paper I)
Sugar J., Musgrove A., 1991, J. Phys. Chem. Ref. Data 20, 859
Zeippen C.J., Butler K., Le Bourlot J., 1987, A&A 188, 251